

Kondo lattice and antiferromagnetic behavior in quaternary CeTAl₄Si₂ (T = Rh, Ir) single crystals

Arvind Maurya, R. Kulkarni, A. Thamizhavel and S. K. Dhar*

Department of Condensed Matter Physics and Materials Science,

Tata Institute of Fundamental Research, Homi Bhabha Road, Colaba, Mumbai 400 005, India.

D. Paudyal

*The Ames Laboratory, U.S. Department of Energy,
Iowa State University, Ames, Iowa 50011-3020, USA.*

(Dated: September 10, 2024)

We report the synthesis and the magnetic properties of single crystalline CeRhAl₄Si₂ and CeIrAl₄Si₂ and their non magnetic La-analogs. The single crystals of these quaternary compounds were grown using Al-Si binary eutectic as flux. The anisotropic magnetic properties of the cerium compounds were explored in detail by means of magnetic susceptibility, isothermal magnetization, electrical resistivity at ambient and applied pressures up to 12.6 kbar, magnetoresistivity and heat capacity measurements. Both CeRhAl₄Si₂ and CeIrAl₄Si₂ undergo two antiferromagnetic transitions, first from the paramagnetic to an antiferromagnetic state at $T_{N1} = 12.6$ K and 15.5 K, followed by a second transition at lower temperatures $T_{N2} = 9.4$ K and 13.8 K (inferred from the peaks in the heat capacity), respectively, in conformity with an earlier report in the literature. The paramagnetic susceptibility is highly anisotropic and its temperature dependence in the magnetically ordered state suggests the *c*-axis to be the relatively easy axis of magnetization. Concomitantly, isothermal magnetization at 2 K along the *c*-axis shows a sharp spin-flop transition accompanied by a sizeable hysteresis, while it varies nearly linearly with field along the [100] direction up to the highest field 14 T of our measurement. The electrical resistivity provides evidence of the Kondo interaction in both compounds, inferred from its $-lnT$ behavior in the paramagnetic region and the decrease of magnetic transition temperature with pressure. The heat capacity data confirm the bulk nature of the two magnetic transitions in each compound, and further support the presence of Kondo interaction by a reduced value of the entropy associated with the magnetic ordering. From the heat capacity data below 1 K, the coefficient of the linear term in the electronic heat capacity, γ , is inferred to be 195.6 and 49.4 mJ/mol K² in CeRhAl₄Si₂ and CeIrAl₄Si₂, respectively classifying these materials as moderate heavy fermion compounds. The main features of the magnetoresistivity measured at a particular temperature correlate nicely with the isothermal magnetization at the same temperature in these two isostructural compounds. We have also carried out an analysis of the magnetization based on the point charge crystal electric field model and derived the crystal electric field energy levels which reproduce fairly well the peak seen in the Schottky heat capacity in the paramagnetic region. Further, we have also performed electronic structure calculations using (LSDA +U) approach, which provide physical insights on the observed magnetic behaviour of these two compounds.

PACS numbers: 81.10.Fq, 75.50.Ee, 75.30.Kz, 75.10.Dg, 71.70.Ch, 75.50.Ee

I. INTRODUCTION

Recently, the synthesis and magnetic properties of quaternary EuTAl₄Si₂ (T = Rh and Ir) single crystals, using the Al-Si binary eutectic as flux have been reported^{1,2}. The two Eu compounds initially order into an incommensurate amplitude modulated antiferromagnetic state at $T_{N1} = 11.7$ and 14.7 K respectively, followed by a second transition to an equal moment state at lower temperature T_{N2} . Though these two compounds prima-facie are antiferromagnetic, the isothermal magnetization curves at low temperatures (below T_{N2}) show a hysteresis right near the origin with a remanance; unlike any other antiferromagnetic material. The EuTAl₄Si₂ compounds adopt an ordered derivative of the ternary KCu₄S₃-type tetragonal, *tP8*, *P4/mmm* structure, which leads to quaternary and truly stoichiometric

1:1:4:2 compounds, with a local fourfold axial (*4/mmm*) symmetry at the Eu site. These are a new addition to several quaternary rare earth-based compounds already known in the literature with 1:1:4:2 stoichiometry, which have been grown using aluminum as flux; for example, RNiAl₄(Ni_xSi_{2-x}), EuNiAl₄Si₂, RNiAl₄Ge₂, RAuAl₄Ge₂ and RAuAl₄(Au_xGe_{1-x})₂ where R is a rare earth metal^{3,4}. While most of these compounds adopt the rhombohedral YNiAl₄Ge₂-type structure⁵, the phases RAuAl₄(Au_xGe_{1-x})₂ and EuAu_{1.95}Al₄Ge_{1.05} crystallize in the KCu₄S₃-type structure⁵. Both structure types are characterized by the slabs of “AuAl₄X₂ (X = Si or Ge)” or “AuAl₄(Au_xGe_{1-x})₂” stacked along the *c*-axis with layers of R atoms in between. The Ce atoms in both CeAuAl₄Ge₂ and CeAuAl₄(Au_xGe_{1-x})₂ ($x = 0.4$) have been reported to be in a valence fluctuating state³. This suggests the possibility of strong hybridization between the Ce-4*f*-orbitals and the itin-

erant electrons in these structure-types, which is known to lead to a variety of anomalous ground states, such as Kondo lattices, heavy fermions with huge effective electron masses, magnetically ordered states with reduced saturation moments^{6,7}. The Néel temperature in some heavy fermion, antiferromagnetic Kondo lattices can be tuned to zero using pressure as an external parameter, which leads to a quantum phase transition where the Fermi-Landau description of quasiparticles breaks down⁸. It was therefore of interest to explore the formation of other RTAl_4Si_2 ($T = \text{Rh}$ and Ir) compounds, in particular for $R = \text{Ce}$. We have been able to grow the single crystals for $R = \text{Ce}$ and Pr and in this report we give a detailed description of properties of two Ce compounds, using the techniques of magnetization, electrical resistivity in zero and applied magnetic fields, and under externally applied pressure, and heat capacity. We find that both $\text{CeTAl}_4\text{Si}_2$ ($T = \text{Rh}$ and Ir) compounds are dense Kondo lattice antiferromagnets, each undergoing two magnetic transitions like the Eu -analogs. We have supplemented our experimental data with electronic structure calculations for $\text{CeTAl}_4\text{Si}_2$ ($T = \text{Rh}$, Ir and Pt) employing the local spin density approximation including Hubbard U -onsite electron-electron correlation.

While this manuscript was under preparation, Ghimire *et al.*⁹ have reported the anisotropic susceptibility and resistivity, and the low temperature heat capacity (1.8 to 30 K) of $\text{CeMAl}_4\text{Si}_2$ ($M = \text{Rh}$, Ir , Pt) compounds⁹. Our observation of two antiferromagnetic transitions in these two compounds ($M = \text{Rh}$ and Ir) is in conformity with their results. Ghimire *et al.* allude to the presence of Kondo interaction and the opportunity to explore strongly correlated electron behaviour in these quaternary compounds. Our low temperature heat capacity data (below 1 K) reveal moderately heavy electron masses. Our more extensive magnetization data, and magnetoresistivity reveal some additional features in the properties of the these two compounds. Our resistivity data at ambient pressure show the presence of Kondo interaction in these compounds, further supported by the resistivity data under externally applied pressure, where we observe a suppression of T_N with pressure, which is a standard feature of Ce -Kondo lattices predicted by the Doniach's phase diagram¹⁰. In a more recent paper, using powder neutron diffraction, Ghimire *et al.*¹¹ have determined that the antiferromagnetic structure in both $\text{CeRhAl}_4\text{Si}_2$ and $\text{CeIrAl}_4\text{Si}_2$ is A-type with propagation vector $\mathbf{k} = (0, 0, 1/2)$ along the \mathbf{c} -axis.

II. EXPERIMENT

The single crystals of $\text{CeTAl}_4\text{Si}_2$ and $\text{LaTAl}_4\text{Si}_2$ were grown by following the same experimental protocol as described in ref. 1 for the Eu -compounds. Their Laue patterns were recorded using a Huber Laue diffractometer, while the phase purity was inferred from the powder x-ray diffraction pattern collected using a PAN-

alytical x-ray diffractometer. The stoichiometry was checked by semiquantitative analysis performed by energy dispersive analysis by x-rays (EDAX). Well oriented crystals were cut appropriately by an electric discharge cutting machine for direction dependent measurements. The magnetization data were measured in a Quantum Design Superconducting Quantum Interference Device (SQUID) magnetometer and Vibration Sample Magnetometer (VSM) in the temperature range 1.8 to 300 K and fields up to 14 T. The electrical resistivity, magnetoresistivity and the heat capacity were measured in a Quantum Design Physical Properties Measurement System (PPMS). Heat capacity measurements down to 100 mK were performed using the dilution insert of QD-PPMS. A piston-cylinder type pressure cell fabricated from MP35N alloy was used to measure the resistivity upto 12.6 kbar. A teflon capsule covering sample platform, holding two samples and one Sn wire as manometer, was filled with Daphne oil, which is hydrostatic pressure medium. The dimension of capsule is such that it fits exactly inside the 5 mm bore of the cell. A feed through made out of beryllium copper alloy was used for providing electrical contacts to the sample and Sn manometer. A cernox temperature sensor and a heater in the form of manganin wire mounted over the cell were fed to a Cryocon PID temperature controller. A 5 mA dc current derived from Keithley current source was passed through samples and the generated voltage was read out by a sensitive nanovoltmeter. All the resistivity measurements were done in the standard four probe configuration. Temperature controller, current source and voltmeter were interfaced to a computer via GPIB and data acquisition was automated by a Labview programme.

III. RESULTS AND DISCUSSION

A. Structure

The compositions obtained from EDAX analysis confirmed the stoichiometric ratio of 1:1:4:2 to within 1 at.% for each element. The powder x-ray diffraction patterns of $\text{CeTAl}_4\text{Si}_2$ ($T = \text{Rh}$ and Ir) are similar to those of Eu -analogs, and no extra peaks due to any parasitic phases were found. A Rietveld refinement using FullProf soft-

TABLE I: Lattice constants a and c , and unit cell volume V of $\text{CeRhAl}_4\text{Si}_2$ and $\text{CeIrAl}_4\text{Si}_2$ as determined from the x-ray powder diffraction pattern.

| | a (Å) | c (Å) | V (Å ³) |
|------------------------------|------------|------------|--------------------------|
| $\text{CeRhAl}_4\text{Si}_2$ | 4.223(2) | 8.048(2) | 143.54(2) |
| $\text{CeIrAl}_4\text{Si}_2$ | 4.236(3) | 8.043(2) | 144.34(2) |

ware¹² based on the $\text{EuIrAl}_4\text{Si}_2$ -type tetragonal crystal structure was performed. The obtained lattice parameters a and c are listed in Table I and are in good agree-

ment with the values reported in ref. 9. It may be noted that similar to Eu compounds¹ the lattice parameter a is larger but c is slightly shorter in Ir analog compared to that of Rh analog but overall the unit cell volume of CeIrAl₄Si₂ is slightly larger than that of the Rh-analog, which is in accordance with the larger atomic volume of Ir.

B. Magnetic susceptibility and magnetization

The magnetic susceptibility, $\chi(T)$, of CeRhAl₄Si₂ and CeIrAl₄Si₂ below 300 K is shown in the main panel of Figs. 1 (a) and 1 (b), for field (0.3 T) applied along the [100] and [001] directions, respectively. The inverse susceptibility in the temperature range 1.8 to 300 K is plotted in the insets of Fig. 1(a) and (b). The susceptibility is highly anisotropic in the paramagnetic region in both compounds and a fit of the Curie-Weiss law, $\chi = \frac{C}{T-\theta_p}$ to the high temperature data (100-300 K), represented by the solid lines, furnishes the Curie-Weiss parameters which are listed in Table II. The effective moments are close to the Ce³⁺-free ion moment value of 2.54 μ_B /Ce. The highly anisotropic nature of the susceptibility is clearly reflected by the respective values of paramagnetic Curie temperature θ_p which are more than one order of magnitude larger for $H \parallel [100]$ in both compounds. In conformity with the trivalent nature of the Ce ions, the compounds order antiferromagnetically at $T_{N1} = 13.3$ and 16 K, and $T_{N2} = 9.4$ and 13.8 K for T = Rh and Ir, respectively, close to the values reported in ref. 9. It may be noted that the absolute value of the polycrystalline averaged θ_p (-100 and -68 K) is substantially higher than T_{N1} . We believe it to be primarily due to the crystal electric field and anisotropic Kondo interaction (*vide infra*) which contribute negatively to θ_p . In the simplest collinear two-sublattice antiferromagnet, the χ_{\perp} along the hard direction is temperature independent below T_N while χ_{\parallel} gradually decreases to zero as $T \rightarrow 0$. A weak temperature dependence of χ along [100] in the two compounds indicates a hard ab -plane.

It may be noted that the anisotropy in $\chi_{[100]}$ and $\chi_{[001]}$ persists in our data(Figs. 1a and 1b) upto 300 K. On the other hand in ref. 9 the two cross each other near 275 K in CeIrAl₄Si₂. Such a crossover, *prima-facie* indicates a change in the easy axis of magnetization with temperature. However, in the crystal electric field analysis of the magnetization data (*vide infra*), the values of the dominant CEF parameter B_2^0 are negative in both compounds and comparable making the anisotropic crossover along the crystallographic axis unlikely.

The magnetic field dependence of susceptibility (M/H) below T_{N1} was investigated at a few fields and the data are plotted in Figs. 1(c-f). The T_N decreases as the applied field is increased, as commonly observed in antiferromagnets. However, the decrease is more substantial for $H \parallel [001]$ which is relatively the easy axis of magnetization. The magnetization in both compounds at

TABLE II: Effective moment and paramagnetic Curie temperature in CeRhAl₄Si₂ and CeIrAl₄Si₂ along the principal crystallographic directions.

| | CeRhAl ₄ Si ₂ | | CeIrAl ₄ Si ₂ | |
|---------------------|-------------------------------------|----------------------|-------------------------------------|----------------------|
| | $\mu_{\text{eff}}(\mu_B/f.u.)$ | $\theta_p(\text{K})$ | $\mu_{\text{eff}}(\mu_B/f.u.)$ | $\theta_p(\text{K})$ |
| $H \parallel [100]$ | 2.65 | -155 | 2.62 | -140 |
| $H \parallel [001]$ | 2.35 | 7.1 | 2.43 | 4 |

T_{N2} exhibits hysteresis thereby indicating that the transition at T_{N2} has a first order character (Figs. 1e-f). The hysteresis is weaker at lower fields and it increases with increment in magnetic field till spin flop field. The change in T_{N1} and T_{N2} with field applied along [100] and [001] directions has been summarized in the phase diagrams shown in Figs. 1g and 1h. Critical points obtained from isothermal magnetization *vs.* magnetic field (MH), electrical resistivity as a function of field (RH) and temperature (RT) measurements are also shown which are in consonance with each other. It may be noted that the phase boundary separating two antiferromagnetic states AF1 and AF2 for $H \parallel [001]$ is of first order character as inferred from the susceptibility and magnetoresistivity data. Also, T_{Ns} suppress faster for field applied along the easy axis *viz.* [001].

The isothermal magnetization at 2 K is linear up to 14 T along [100] while there is a sharp spin-flop (metamagnetic-like) transition revealed by two closely spaced jumps in the magnetization along the [001]-direction beginning at 5.3(6.4) T for CeRh(Ir)Al₄Si₂ (see Figs. 2a and 2b). The former behaviour is typical of an antiferromagnet when the moments are perpendicular to the field. The field dependence thus clearly marks the easy and the hard-axes of magnetization. This is in conformity with neutron diffraction in which magnetic moments aligned antiferromagnetically along the c -axis below T_{N2} is inferred¹¹. The magnetization attains a value of 0.95 and 1.14 μ_B /Ce at 14 T along the c -axis in CeRhAl₄Si₂ and CeIrAl₄Si₂ respectively, which is lower than the saturation moment of Ce³⁺ (2.14 μ_B /Ce). We attribute the lower values to the combined effects of crystal electric field and partial quenching of the Ce moments due to Kondo screening. We note that the magnetization at 14 T at 2 K is lower in the Rh-analogue, which is consistent with its higher Kondo temperature, T_K (*vide infra*). The magnetization at 2 K in 14 T is not yet saturated and is lower than the values determined in ref. 11.

One can observe a clear hysteresis in the vicinity of spin-flop transition. The hysteretic behaviour is also observed in the temperature dependence of magnetic susceptibility (mentioned above) and electrical resistivity (*vide infra*), revealing the presence of first order field induced effect. The spin-flop field value and the magnetization decrease with the increase of temperature. The magnetization for $H \parallel [100]$ is relatively insensitive to the variation in temperature as inferred from Figs. 2(c)

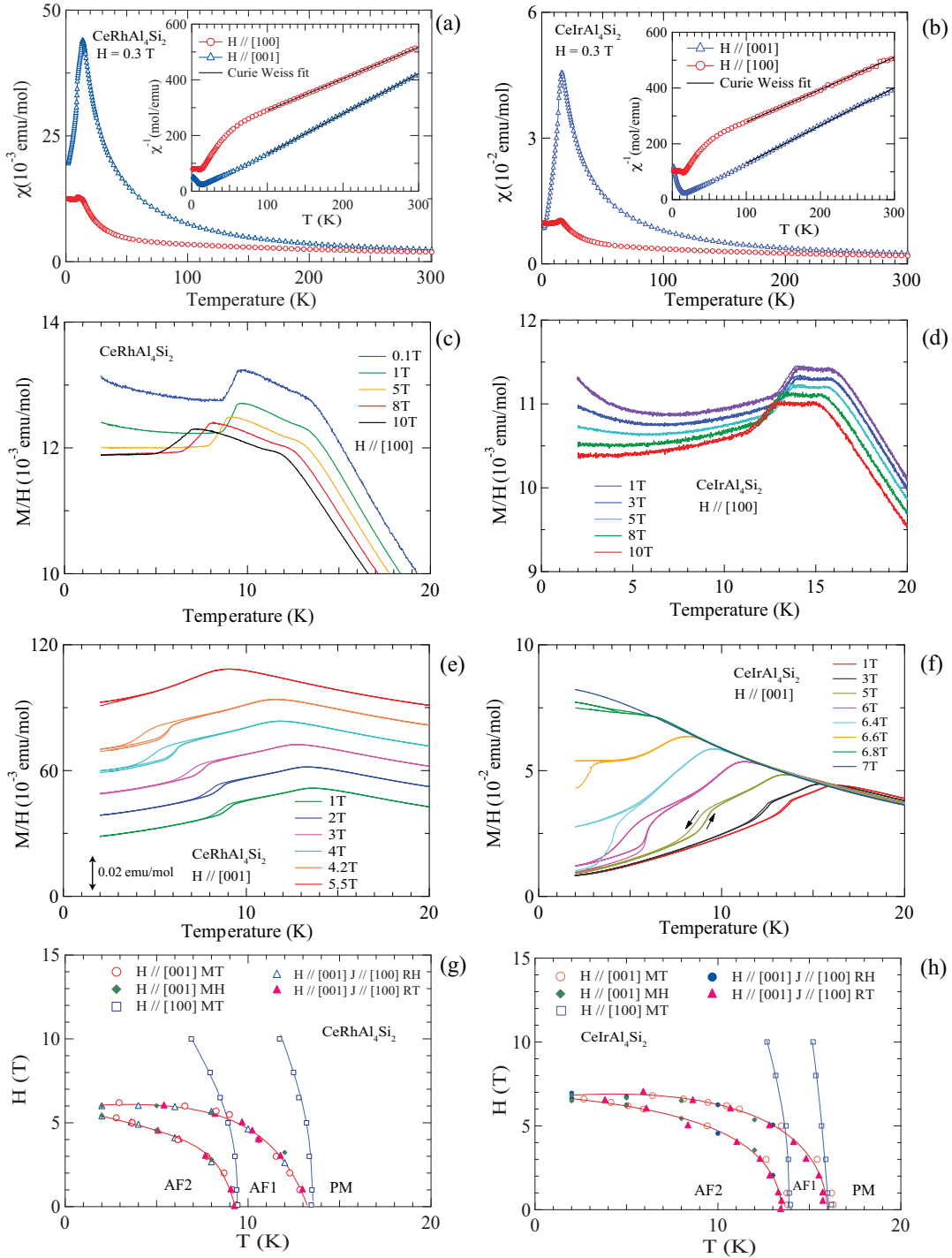


FIG. 1: (Color online) Magnetic susceptibility and inverse susceptibility (in inset) up to 300 K of (a) CeRhAl₄Si₂ and (b) CeIrAl₄Si₂. The dependence of M/H on field is shown in (c-f) for $H \parallel [100]$ and $H \parallel [001]$, respectively. In (e) and (f) single color plots show ZFC (zero field cooled), FCC (field cooled cooling) and FCH (field cooled heating) data revealing field induced first order nature of transition at T_{N2} . Magnetic phase diagrams of (g) CeRhAl₄Si₂ and (h) CeIrAl₄Si₂ derived from magnetization (MT, MH) and magnetoresistivity (RT, RH) data (*vide infra*). AF1, AF2 and PM represents two antiferromagnetic and paramagnetic phases, respectively.

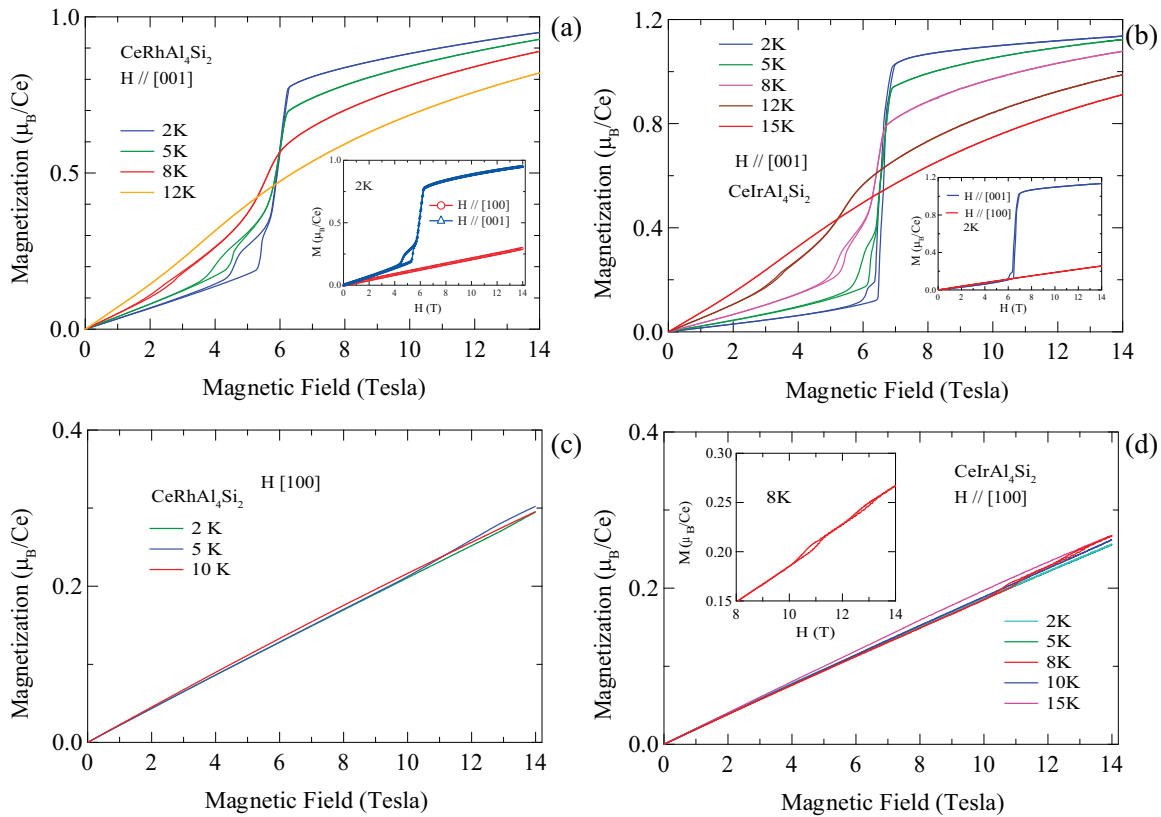


FIG. 2: (Color online) Isothermal magnetization curves at selected temperatures for (a) $\text{CeRhAl}_4\text{Si}_2$ and (b) $\text{CeIrAl}_4\text{Si}_2$ along [001] direction. The insets show the data at 2 K for $H \parallel [001]$ and $H \parallel [100]$. (c) and (d) show the data at selected temperatures for $H \parallel [100]$. The inset in (d) reveals two weakly first order changes which are also seen in the magnetoresistance data. (see Fig. 7).

and 2(d). The inset in Fig. 2(d) reveals two weakly hysteretic regions in the magnetization of $\text{CeIrAl}_4\text{Si}_2$ at 8 K.

C. Electrical Resistivity

Figs. 3(a-d) show the zero-field electrical resistivity $\rho(T)$ data of $\text{CeRhAl}_4\text{Si}_2$ (left panels) and $\text{CeIrAl}_4\text{Si}_2$ (right panels) for the current density J parallel to [001] and [100] directions, respectively. The corresponding data for the non-magnetic La-reference compounds are also plotted. While anomalies at T_{N1} and T_{N2} for $J \parallel [001]$ are visible either in the ρ vs T or $d\rho/dT$ vs T plots (not shown), the ρ for $J \parallel [100]$ shows a sudden change of slope only at T_{N2} .

There is a considerable anisotropy in the resistivity, ρ along [001] being larger compared to [100] in the entire temperature range. The residual resistivity ratio (RRR) ρ_{300K}/ρ_{2K} is 17.8 and 29.9 for $J \parallel [100]$ and [001], respectively for $\text{CeIrAl}_4\text{Si}_2$, compared to its corresponding values of 3.2 and 3.4 in $\text{CeRhAl}_4\text{Si}_2$. While our RRR for $\text{CeIrAl}_4\text{Si}_2$ is comparable to the value reported by Ghimire et al⁹, in $\text{CeRhAl}_4\text{Si}_2$ our RRR values are lower for reasons unknown to us. We repeated the measurements on a second sample of $\text{CeRhAl}_4\text{Si}_2$ but observed

similar low values of RRR . Our values of resistivity are also significantly higher than reported in ref. 9. Though our single crystals looked good superficially, there may be micro-voids and micro-cracks which lead to higher observed resistivity. While $\rho_{[001]}$ decreases as the temperature is decreased below 300 K, $\rho_{[100]}$ shows a slight negative temperature coefficient above 100 K. The $4f$ -derived part of the resistivity ρ_{4f} is calculated by subtracting the $\rho(T)$ data of La-analog from the corresponding Ce-compound, which is also shown in Figs. 3(a) and 3(b) and replotted in 3(c) and 3(d) on a semi-logarithmic scale. ρ_{4f} reveals a negative logarithmic temperature dependence along both directions which is a hallmark of the Kondo interaction. The high temperature peak in ρ_{4f} in range 100-200 K, which arises due to the interplay of Kondo interaction and crystal electric field levels, occurs at different temperatures along the two directions. The resistivity data thus reveal that these two Ce-compounds are dense anisotropic Kondo lattice antiferromagnets.

The Kondo behaviour of $\text{CeTAl}_4\text{Si}_2$ compounds, inferred above from the resistivity data at ambient pressure, was probed further by measuring the resistivity under pressure up to 12.6 kbar. According to the standard Doniach phase diagram of a magnetic Kondo lattice, pressure enhances the $4f$ -conduction band coupling

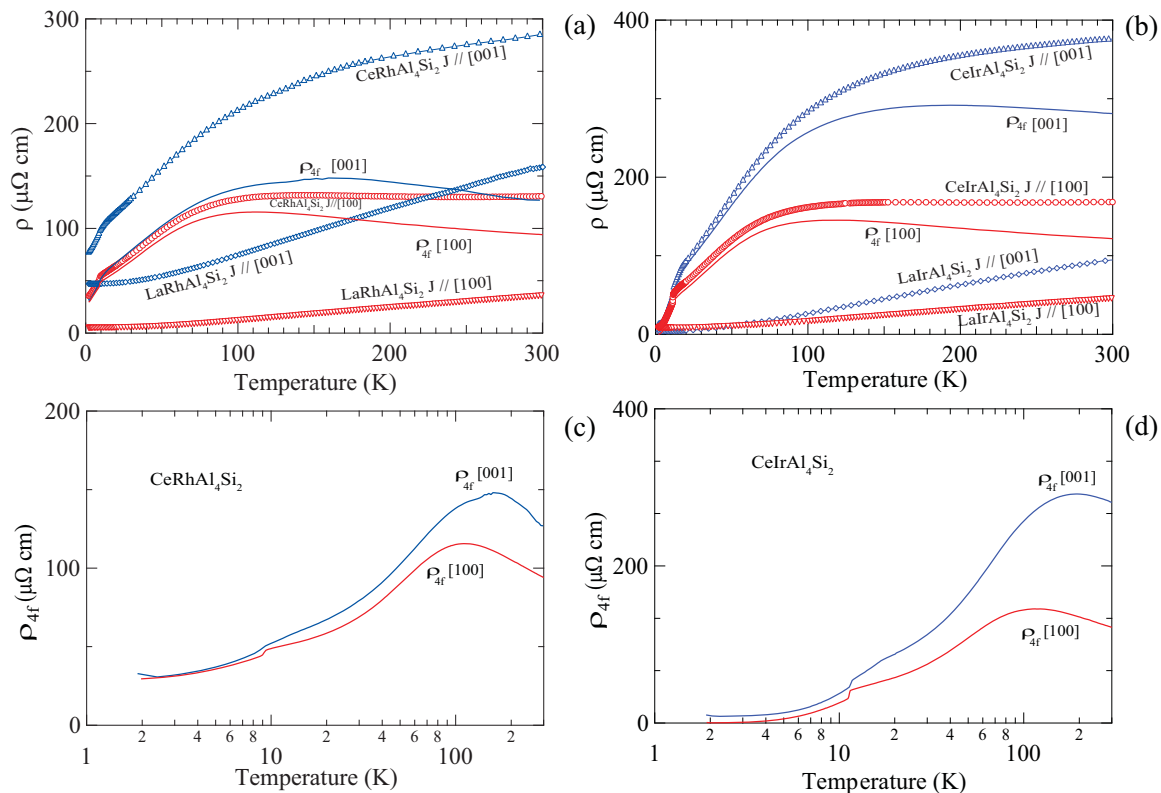


FIG. 3: (Color online) Electrical resistivity of (a) CeRhAl₄Si₂ and LaRhAl₄Si₂; (b) CeIrAl₄Si₂ and LaIrAl₄Si₂ along the major crystallographic directions. ρ_{4f} is represented by solid lines. $\rho_{4f}(T)$ data plotted on logarithmic temperature scale are shown in (e) and (f).

and the Kondo temperature, which decreases the T_N . At sufficiently high pressures when the Kondo interaction dominates over the RKKY interaction, T_N approaches zero leading to a quantum phase transition. Fig. 4 shows the resistivity of the two compounds at selected values of pressure. The pressure cell was simultaneously loaded with the two compounds and numbers in parentheses indicate the order of data acquisition. The T_{N2} in both compounds decreases with pressure, which is qualitatively in consonance with the Doniach phase diagram. T_{N2} decreases from 13.6 (at ambient pressure) to 8.2 (6.2) K at 8.8(11.4) kbar in CeIrAl₄Si₂, while it decreases from 9.4 to 4.7 K at 8.8 kbar in CeRhAl₄Si₂. No apparent anomaly is observed at higher pressures in the two compounds down to 1.8 K both in ρ versus T and $d\rho/dT$ versus T plots. Data at lower temperatures and presumably higher pressures are required to track the eventual decrease of T_{N2} to 0 K.

The resistivity data under pressure were measured up to 300 K and the data for CeRhAl₄Si₂ are shown in Fig. 4c. The temperature T_{max} at which the resistivity attains its maximum value ρ_{max} increases from ~ 108 at ambient pressure to 130 K at 12.6 kbar. Qualitatively, the upward shift of T_{max} is in conformity with the increase of T_K with pressure. The inset of Fig. 4c shows ρ/ρ_{max} scales with T/T_{max} in a reasonably large inter-

val around T_{max} . Such a scaling relationship has been reported in some Kondo compounds¹³. Though T_{max} increases with pressure in the Ir-analogue as well, we observed a substantial difference in the resistivity values particularly at higher temperatures taken at nearly the same pressure in two different runs (without affecting the transition temperature), while as in the Rh compound the resistivity values nearly matched. Therefore, we have not shown the data for the Ir-analogue at higher temperatures. Fig. 4d shows the T-P phase diagram of both compounds. It may be noted that T_{N1} is not discernible in any of our pressure dependent resistivity measurement as the data were taken for $J \parallel [100]$ where we see only one transition (*cf.* Figs. 5c and 5d).

D. Magnetoresistance

The variation of resistivity at selected values of magnetic field at low temperatures is shown in Figs. 5(a-d). For H applied along [100] and $J \parallel [001]$ the resistivity plots are qualitatively similar except that there is a gradual downward shift of T_N with increasing field. In CeIrAl₄Si₂, one sees two steps to the lower temperature transition at fields of 10 and 12 T (Fig. 5b), which is consistent with two weakly first order changes seen in the

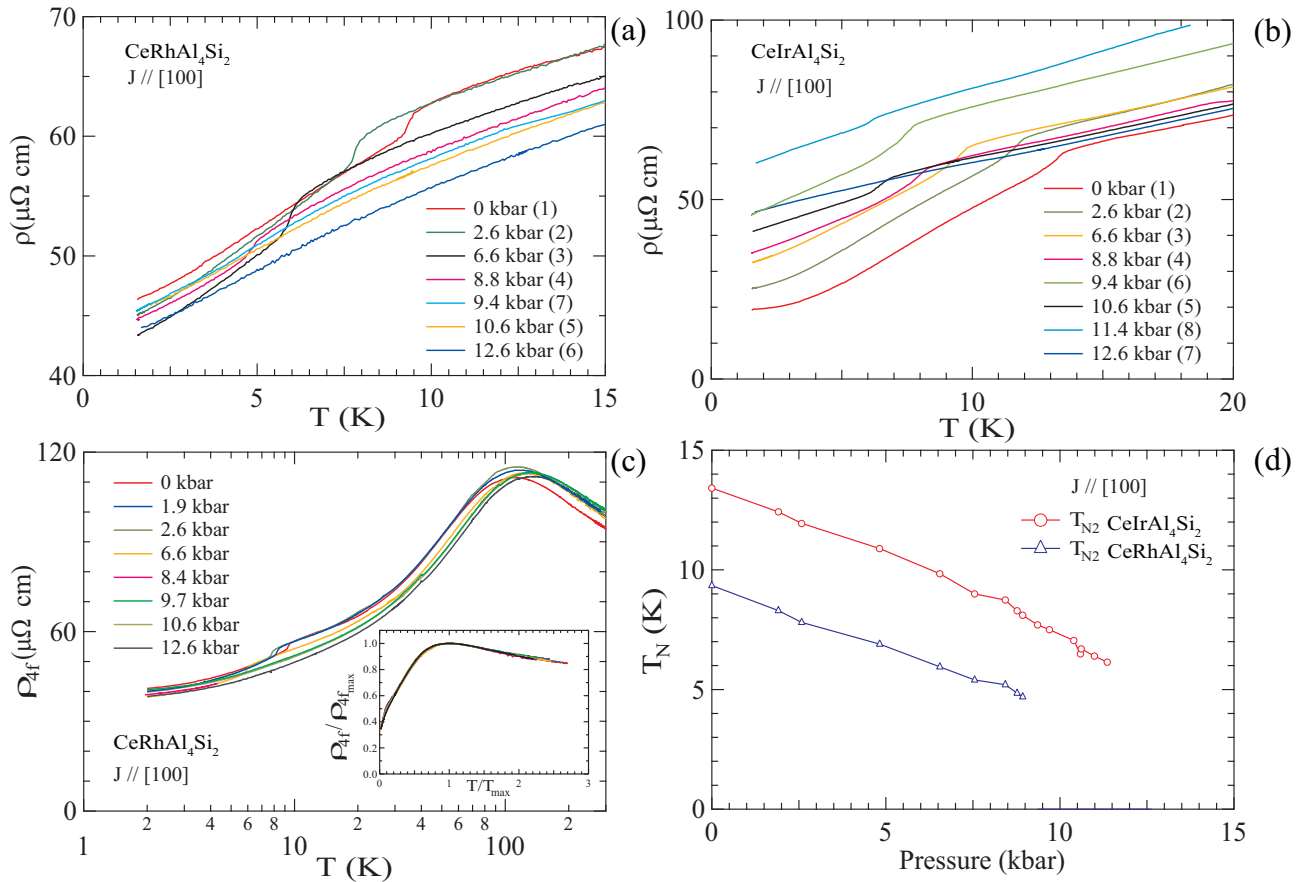


FIG. 4: (Color online) Electrical resistivity under hydrostatic pressure at low temperatures when $J \parallel [100]$ for (a) $\text{CeRhAl}_4\text{Si}_2$, (b) $\text{CeIrAl}_4\text{Si}_2$. Numbers in parenthesis denote the the order in which pressure was applied. (c) $4f$ -derived electrical resistivity of $\text{CeRhAl}_4\text{Si}_2$ upto 300 K on logarithmic temperature scale, (d) variation of T_{N2} with pressure in $\text{CeRhAl}_4\text{Si}_2$ and $\text{CeIrAl}_4\text{Si}_2$ when $J \parallel [100]$.

magnetization (inset, Fig. 2d). On the other hand prominent changes are seen for $H \parallel [001]$ and $J \parallel [100]$. T_N is suppressed relatively faster with a substantial hysteresis in the field-range where spin-flop occurs, revealing first order effects in conformity with the magnetization data. It may be noted that there is a slight kink at 8.6 and 11.2 K in 5.5 T and 6 T in $\text{CeRhAl}_4\text{Si}_2$ and $\text{CeIrAl}_4\text{Si}_2$, respectively. The inset of Fig. 5(d) shows that T_{N1} in 6 T has decreased to the temperature at which the kink occurs in $\text{CeIrAl}_4\text{Si}_2$. Maybe the anomaly is present at lower fields also but it is not discernible. Similar explanation holds in case of $\text{CeRhAl}_4\text{Si}_2$. The inset also shows that there is a good agreement between the hysteresis in the resistivity (on right scale) and M/H (on left scale) data at 6 T field applied parallel to $[001]$.

Magnetoresistivity MR was also probed by varying the field from zero to 14 T at selected temperatures, with the field and current density in various orientations and the results are plotted in Figs. 6 and 7. The magnetoresistance, MR is defined as $MR = [\rho(H) - \rho(0)]/\rho(0)$. With reference to Fig. 6(a) the MR of $\text{CeRhAl}_4\text{Si}_2$ at

2 K for field applied in the ab -hard plane is small and attains a value of $\sim 3\%$ at 14 T. On the other hand for field applied along the easy-axis $[001]$ the MR at its maximum is an order of magnitude larger. Initially the positive MR increases with field, jumps sharply at the first step of the spin-flop attaining a maximum of 30% at nearly the second step and then decreases sharply and becomes negative at higher fields. In the return cycle the MR shows hysteresis in the spin-flop region, which corresponds nicely with the hysteresis in the magnetization (*cf.* Fig. 2). We have reported earlier similar sharp changes in the MR of EuNiGe_3 which is an antiferromagnet with T_N of 13.2 K¹⁴.

For $\text{CeIrAl}_4\text{Si}_2$ the MR for $H \parallel [001]$ is qualitatively similar (Figs. 6 (b) at low fields except that the MR in the spin-flop region is even larger and exceeds 100 %. Above the spin-flop the MR drops sharply but unlike $\text{CeRhAl}_4\text{Si}_2$ it does not attain negative values and remains positive up to the highest field of 14 T. For field applied in the ab -hard plane viz. $J \parallel [100]$ and $H \parallel [010]$; $J \parallel [001]$ and $H \parallel [100]$ the MR is positive qualitatively

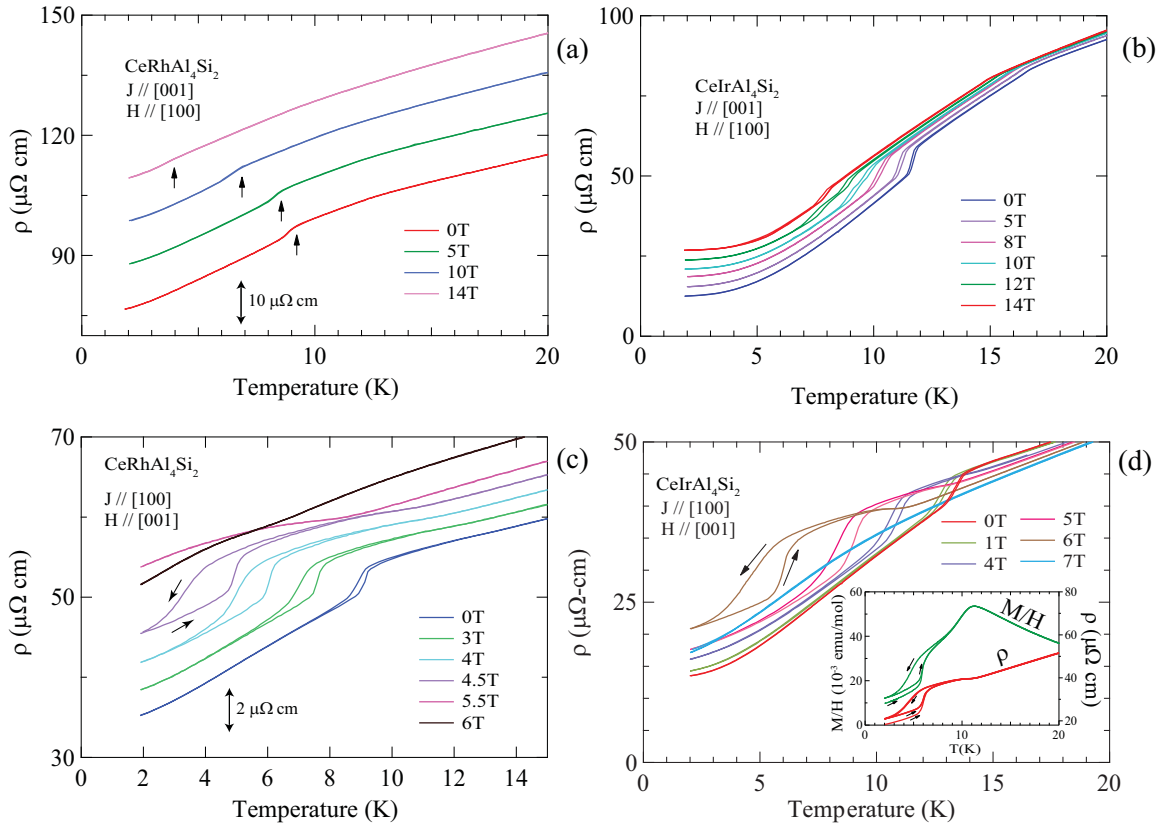


FIG. 5: (Color online) Magnetic field dependence of $\rho(T)$ of $\text{CeRhAl}_4\text{Si}_2$ and $\text{CeIrAl}_4\text{Si}_2$ in different configuration. In (a) and (c) the in-field plots have been shifted upward by a constant offset for clarity.

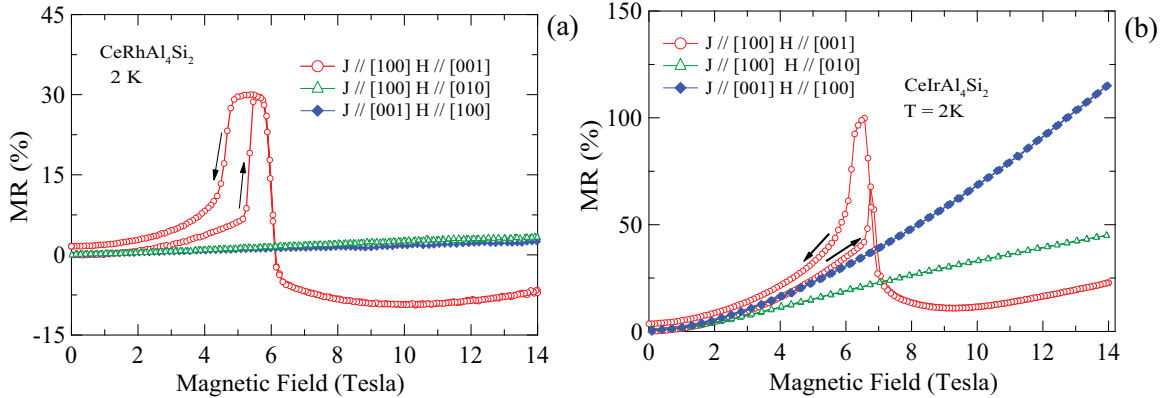


FIG. 6: (Color online) Current and field-direction dependence of isothermal Magnetoresistance (MR) at 2 K upto 14 T of (a) $\text{CeRhAl}_4\text{Si}_2$ and (b) $\text{CeIrAl}_4\text{Si}_2$.

similar the that of $\text{CeRhAl}_4\text{Si}_2$ but its magnitude is much larger. At 2 K the MR rises monotonically reaching 44 and 115 %, respectively at 14 Tesla. The latter value is even larger than the peak value for $H \parallel [001]$. The observed MR can be qualitatively explained by invoking three contributions, i) the MR of an antiferromagnet, ii) the Kondo contribution and iii) the positive contribution due to the cyclotron motion of the conduction electrons. In an antiferromagnet for $T \ll T_N$ when the

field is applied along the easy axis, it tends to suppress the spin fluctuations in one sublattice and increase in the other. Typically, the MR resulting from the combined fluctuations is positive¹⁵. In the spin-flop region the spins can be imagined to be in a canted state with higher spin disorder resistivity. As the field is increased further leading to spin-flip where a saturated paramagnetic state is achieved, the MR becomes negative. A magnetic field tends to suppress the Kondo scattering of

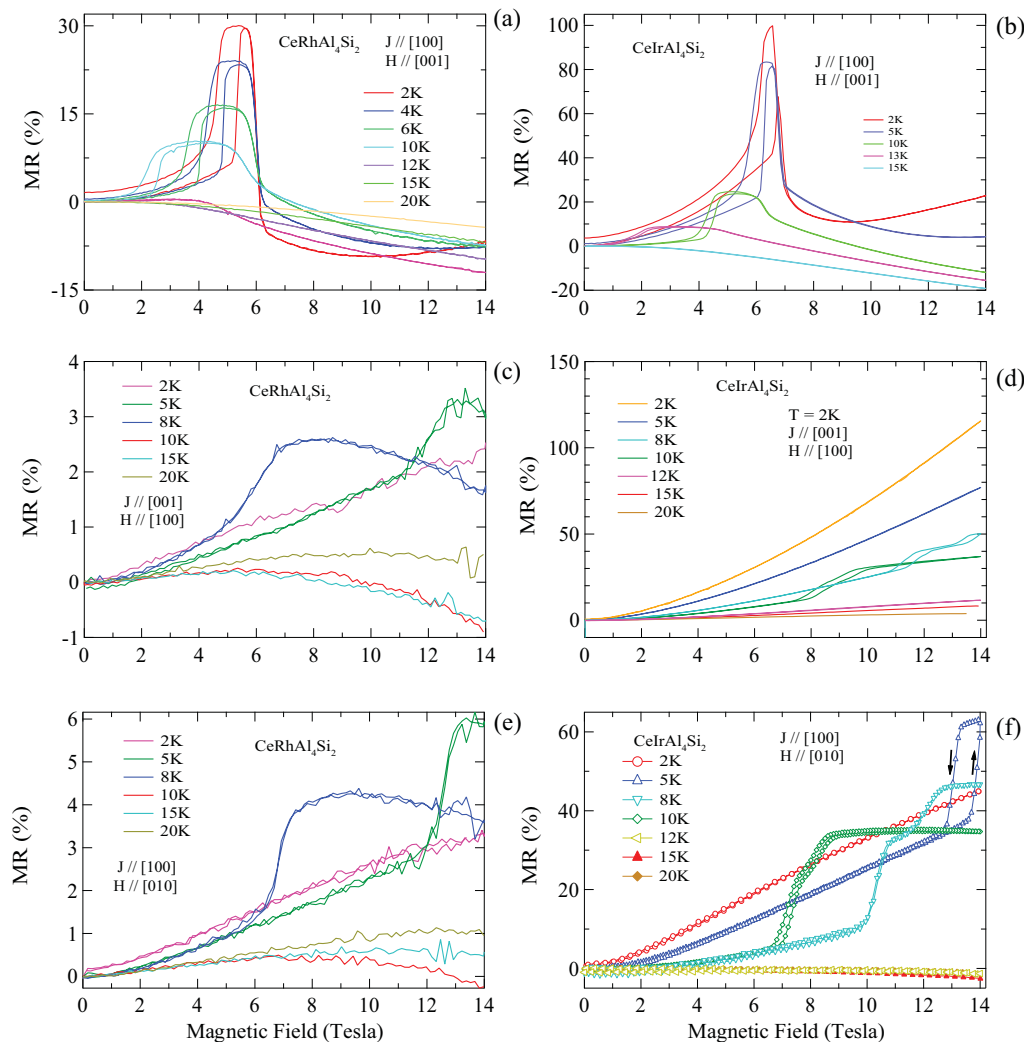


FIG. 7: (Color online) Temperature dependence of $MR(H)$ in CeRhAl₄Si₂ and CeIrAl₄Si₂. The data in (c) and (e) are looking scattered due to the relatively smaller values of the MR .

the conduction electrons leading to a negative MR . According to Zlatic's model, which is based on the single center scattering picture, the MR has a negative minimum at nearly $T = T_K/2$, changes sign at around $T_K/2\pi$ and has a positive maximum at $T = 0$ K¹⁶. Taking a T_K of nearly 10 K for CeRhAl₄Si₂ (*vide infra*) the negative minimum due to Kondo interaction should occur around 5 K. In CeIrAl₄Si₂ with a lower T_K , the negative minimum should occur at even lower temperature. The MR is positive at these temperatures indicating that the contribution due to the effect of magnetic field on the antiferromagnetic state to MR is dominant. The negative MR of CeRhAl₄Si₂ above 6 T may have a contribution from the Kondo interaction while it would be relatively far lower in CeIrAl₄Si₂. As regards the positive contribution from the cyclotron motion of the electrons, in a simple two-band model¹⁷ the MR is proportional to B^2 where B is the field and inversely proportional to $\rho(0)^2$. The resistivities of CeRhAl₄Si₂ and CeIrAl₄Si₂ at 2 K

are 35.26 and 13.53 $\mu\Omega cm$ for $J \parallel [100]$; the ratio decreases with increasing temperature. Therefore, it is expected that the positive cyclotron MR at 2 K will be roughly nine times larger in CeIrAl₄Si₂. We speculate that may be the reason why the MR remains positive in the Ir-analogue at high fields while it is negative in the Rh-analogue.

The sharp upturn in the MR at spin flop and the associated hysteresis shift to lower fields as the temperature is increased (Figs. 7 (a) and 7 (b)). The relatively sharp peak in the MR at 2 K increasingly broadens at higher temperatures, mimicking qualitatively the broadened spin-flop region as the temperature is increased (cf Figs. 2a and 2b). Above the spin flop, qualitatively the MR shows a similar field and temperature dependence in two compounds. As mentioned above the Kondo scattering of the conduction electrons should be partially quenched in a magnetic field leading to negative MR . The effect is maximum close to $T_K/2$ and decreases as

the temperature is increased. It may be noted that at 4, 6 and 10 K the MR in $\text{CeRhAl}_4\text{Si}_2$ in a limited range above 6 T becomes less negative than its corresponding values at 2 K. A negative contribution from the Kondo interaction that decreases as the temperature is increased above T_K may explain this. As the Kondo interaction is relatively weaker in the Ir-analogue, its contribution to MR is not significant enough to cause a similar behaviour in $\text{CeIrAl}_4\text{Si}_2$. Possible differences in the positive MR due to the cyclotron motion of the conduction electrons between the two compounds decrease with the increase of temperature. In the paramagnetic region the applied field will tend to suppress residual spin fluctuations leading to a negative MR as observed at 15 and 20 K in $\text{CeRhAl}_4\text{Si}_2$. Clearly several competing mechanisms are contributing to MR which have slightly different comparative energy scales in the two compounds.

The MR in $\text{CeRhAl}_4\text{Si}_2$ at selected temperatures, for fields applied in the ab -plane, i.e. along [100] and [010] is qualitatively similar for current density parallel to [001] and [100], respectively (see, Figs. 7c and 7e). A relatively sharp upturn in MR is seen at 5 and 8 K around ~ 12 and ~ 6 T, respectively, which is most likely arising from changes in the spin reorientation. In $\text{CeIrAl}_4\text{Si}_2$, for $J \parallel [001]$ and $H \parallel [100]$, we observe two steps with hysteresis at 8 K which correlate well with the data shown in the inset of (Fig. 2(d)). A single step with hysteresis is seen in the 10 K data; however no corresponding anomaly is clearly seen in the magnetization. The MR in $\text{CeIrAl}_4\text{Si}_2$ for $J \parallel [100]$ and $H \parallel [010]$ also shows some peculiar features. A field induced hysteresis appears at 5 K around 13 T, which splits into two at 8 and 10 K at lower fields but vanishes again at 12 K. It may be noted that the ratios of resistivities of the Rh and Ir compounds at 2, 10 and 20 K for J parallel to [001] are nearly 6, 2.4 and 1.2, respectively. As mentioned above the positive MR due to the cyclotron motion is expected to be much larger in the Ir analogue, particularly at low temperatures.

E. Heat Capacity

The heat capacity of $\text{CeRh}(\text{Ir})\text{Al}_4\text{Si}_2$ was measured between 100 mK and 150 K to gain more information about the magnetically ordered Kondo lattice state such as the entropy associated with the magnetic ordering, values of the coefficient of the linear term in the electronic heat capacity γ , which is proportional to enhanced electron effective mass, and Kondo temperature. The heat capacity of nonmagnetic analogs $\text{LaRh}(\text{Ir})\text{Al}_4\text{Si}_2$ was also measured between 2 and 150 K. The data are plotted in Fig. 8. The heat capacity clearly exhibits two peaks in both cerium compounds (Figs. 8 (a) and 8(b)) confirming the occurrence of two bulk phase transitions. The peak temperatures are overall in good agreement with the corresponding peaks in the susceptibility. For $\text{CeIrAl}_4\text{Si}_2$ the heat capacity was also measured in 5 and 8 T. The

two peaks shift to lower temperatures in 5 T and they virtually disappear in 8 T above the spin-flop field where the field induces a saturated paramagnetic state.

The heat capacity data of La analog is typical of a non-magnetic reference compound. The plots of C/T vs. T^2 below 5 K for the two La-compounds (not shown) are linear and a fit of the standard expression $C/T = \gamma + \beta T^2$, where γ and β are the electronic and phononic part of the heat capacity, furnishes the following values, $\gamma = 8.7$ and 8.0 mJ/mol K², $\beta = 0.22$ and 0.21 mJ/mol K⁴ for the Rh and Ir compounds, respectively. Our values of γ and β are comparable with those reported in ref. 9. The $4f$ -derived entropy S_{4f} was calculated by the following relation:

$$S_{4f} = \int \frac{C_{4f}}{T} dT \quad (1)$$

where C_{4f} was obtained by subtracting the heat capacity of the La-analog from the corresponding Ce-compound and making the usual assumption of lattice heat capacity being identical for the isotypic La and Ce compounds. Only 64% (72%) of entropy S_{4f} for a doublet ground state with effective spin 1/2 (i.e. $Rln2$) is released up to T_{N1} for $\text{CeRh}(\text{Ir})\text{Al}_4\text{Si}_2$ indicating the presence of Kondo interaction in these materials, assuming insignificant short range order above T_{N1} . The entropy corresponding to full doublet ground state is recovered at temperature ~ 32 K (31 K).

The Kondo behavior of resistivity together with the reduced value of entropy at the magnetic transition temperature T_m imply a partial quenching of the $4f$ -derived Ce magnetic moment by the Kondo interaction. In such cases the degeneracy of the ground state doublet is partially removed by the Kondo effect, and it has been shown that $S_{4f}(T_m) = S_K(T_m/T_K)$, where S_{4f} is the entropy associated with the magnetic ordering and S_K is the entropy at T_m due to the Kondo effect with the Kondo temperature of T_K ¹⁸. The specific heat and the entropy as a function of T/T_K for a spin 1/2 Kondo impurity is known¹⁹, and the ratio T_m/T_K can be determined using the value of S_{4f} . Using this procedure we get a single-ion Kondo temperature T_K of 14 and 10 K in $\text{CeRhAl}_4\text{Si}_2$ and $\text{CeIrAl}_4\text{Si}_2$, respectively. On the other hand if T_m is taken as the temperature at which the upturn in the heat capacity begins than T_K of 12.3 and 7.7 K are obtained. We would like to emphasize that this procedure assumes negligible short range order above the magnetic transition and may therefore overestimate the Kondo temperature. The Kondo temperature of a lattice is believed to be lower than its value for a single impurity. The simple analysis presented here supports the picture of two magnetically ordered compounds with a residual weak Kondo interaction with a Kondo temperature lower or comparable (in the case of Rh-analog) to the magnetic ordering temperature. It may also be noticed that the T_K of the Ir compound is lower than that of the Rh analog. This suggests larger electron correlation effect in $\text{CeRhAl}_4\text{Si}_2$, which is amply confirmed by the low temperature heat

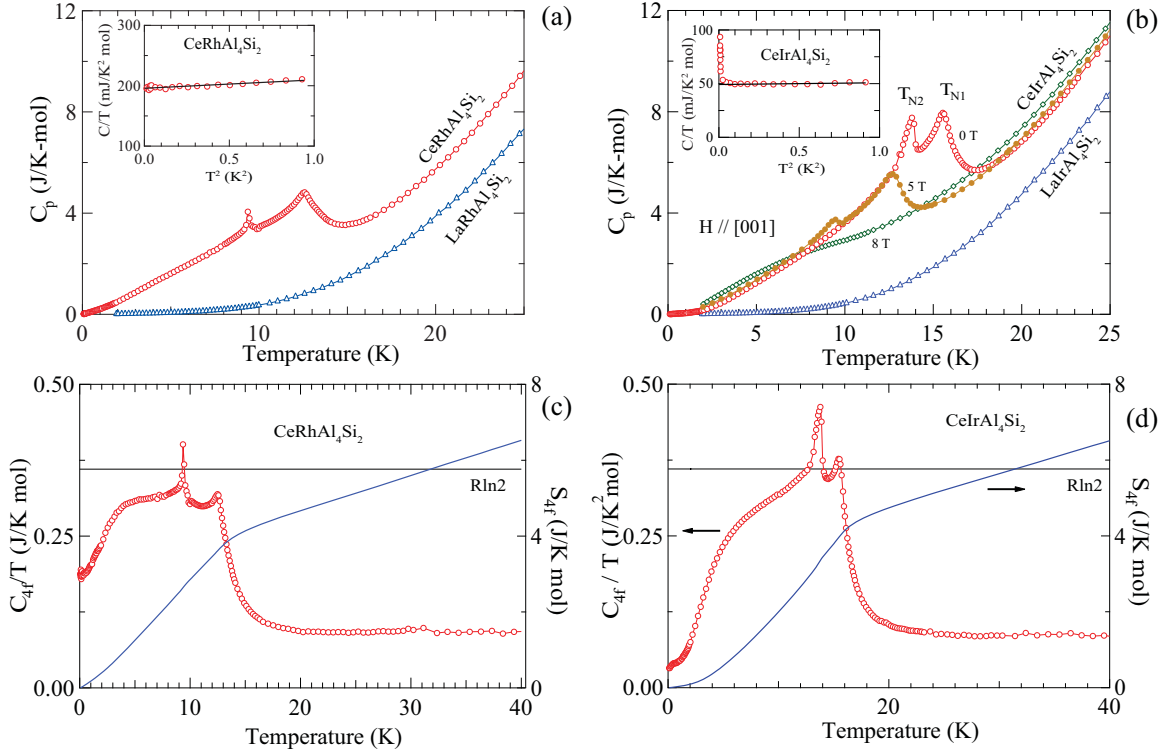


FIG. 8: (Color online) Heat capacity and calculated entropy as a function of temperature of $\text{CeRhAl}_4\text{Si}_2$ (left panels) and $\text{CeIrAl}_4\text{Si}_2$ (right panels). The heat capacity of La analogs are also plotted. The inset in (a) and (b) show the low temperature data of Ce compounds as C/T vs. T^2 .

capacity data discussed below.

The heat capacity below 1 K down to 100 mK, plotted as C/T versus T^2 is shown in the insets of Figs. 8(a) and (b). An extrapolation of the data to $T = 0$ K gives $\gamma = 195.6$ and 49.4 mJ/mol K^2 in the Rh and its Ir-sibling. The values of γ are an order of magnitude larger than the corresponding values in the La-analog and imply a moderate enhancement of the effective electron masses due to the residual Kondo interaction in these two compounds. The upturn in C/T of $\text{CeIrAl}_4\text{Si}_2$ at very low temperatures is attributed to the nuclear Schottky heat capacity arising from the Ir hyperfine quadrupolar interaction.

The $4f$ -derived part of the heat capacity in the paramagnetic state in both $\text{CeRh}(\text{Ir})\text{Al}_4\text{Si}_2$ shows a broad hump at around 70-80 K indicating a Schottky anomaly due to the splitting of $2J + 1$ degenerate levels. This Schottky anomaly is discussed in the next section.

F. Crystalline Electric Field Analysis

The experimental data presented above show unequivocally that $\text{CeTAl}_4\text{Si}_2$ ($T = \text{Rh}, \text{Ir}$) compounds undergo antiferromagnetic ordering at low temperatures. Furthermore, the magnetization measurements revealed a reduced moment of $\sim 1 \mu_B/\text{Ce}$ which is much less compared to the free ion value of $g_J J (= 6/7 \times 5/2)$, $2.14 \mu_B/\text{Ce}$.

This fact together with a large negative paramagnetic Weiss temperature θ_p , the negative logarithmic increase of resistivity, reduced heat capacity jump and a relatively large Sommerfeld coefficient, clearly indicate significant influence of Kondo and crystal electric field (CEF) effects. To gain more understanding of the magnetic behaviour of these compounds, we have performed a CEF analysis on the magnetization and heat capacity data based on a point charge model. The Ce-atom in $\text{CeTAl}_4\text{Si}_2$ occupies the $1b$ -Wyckoff's position and hence possesses the $4/mmm$ (\mathcal{D}_{4h}) tetragonal point symmetry. For half integral spin of $J (= 5/2)$, the crystal field potential will split the $2J + 1 (= 6)$ degenerate levels into three doublets. The CEF Hamiltonian for the Ce-atom in a tetragonal site symmetry is given by,

$$\mathcal{H} = B_2^0 O_2^0 + B_4^0 O_4^0 + B_4^4 O_4^4, \quad (2)$$

where B_i^m and O_i^m are the CEF parameters and the Stevens operators, respectively^{20,21}. Here we have ignored the 6-th order Stevens operators in the Hamiltonian as they are zero for $J = 5/2$.

In the molecular field approximation, the total susceptibility χ is expressed in terms of the CEF susceptibility $\chi_{\text{CEF}i}$ and the molecular field constant λ as,

$$\frac{1}{\chi_i} = \frac{1}{\chi_{\text{CEF}i}} - \lambda_i. \quad (3)$$

TABLE III: Crystal field parameters, molecular field constant and the energy levels for CeTAl₄Si₂ (T = Rh and Ir) obtained from the CEF fitting to the inverse susceptibility plot

| | CeRhAl ₄ Si ₂ | CeIrAl ₄ Si ₂ |
|-----------------------------|-------------------------------------|-------------------------------------|
| B_2^0 (K) | -6.52 | -1.40 |
| B_4^0 (K) | -0.63 | -0.43 |
| B_4^4 (K) | 4.74 | 6.34 |
| $\lambda_{[100]}$ (mol/emu) | -122 | -126 |
| $\lambda_{[001]}$ (mol/emu) | -45 | -5 |
| Δ_1 (K) | 136 | 120 |
| Δ_2 (K) | 342 | 361 |

The χ_{CEF_i} is given by the standard susceptibility expression, by the combination of Curie term and the Van-veleck term²². It is to be mentioned here that the effective moment μ_{eff} along both the directions are slightly deviated from the standard value of 2.54 μ_{B} /Ce, for a cerium atom in its trivalent state. Hence, while performing CEF analysis on the magnetic susceptibility data, we have plotted the inverse susceptibility plot in the form of $1/(\chi - \chi_0)$, where χ_0 is determined from the modified Curie-Weiss law: $\chi = \chi_0 + C/(T - \theta_p)$ by fixing the effective magnetic moment to 2.54 μ_{B} /Ce. A similar kind of approach has been made on previous occasions as well^{23,24}. Figs. 9(a) and (b) show the calculated CEF magnetic susceptibility which explains the anisotropy reasonably well at high temperatures but deviates from the experimental data at low temperatures. Similar quality of fits has earlier been seen, for example, in CeCu₂ and CeAgSb₂^{25,26}. Although it is possible to achieve a better fit to the experimental data, we have chosen the crystal field parameters in such a way that the corresponding crystal field energy levels obtained by diagonalizing the crystal field Hamiltonian (Eq. 2) explain the Schottky heat capacity to be discussed later. The crystal field parameters, molecular field constants and the crystal field split energy levels are listed in Table III. It is to be noted here that the molecular field constant λ is very large and highly anisotropic similar to that of the paramagnetic Weiss temperature θ_p as mentioned earlier. This large value of the molecular field λ may be attributed to anisotropic magnetic exchange interactions and due to Kondo effect. Large values of λ have, for example, been reported in Kondo antiferromagnets CeCu₂ ($\lambda = 70$ mol/emu), CeIrIn₅ ($\lambda = -62$ mol/emu), CeRhIn₅ ($\lambda = -36$ mol/emu) and CeAgSb₂ ($\lambda_{[100]} = -28$ mol/emu)²⁵⁻²⁷. The negative value of λ_i in CeTAl₄Si₂ implies the antiferromagnetic interaction of

the Ce-4f moments in these compounds.

We have also calculated the isothermal magnetization based on the CEF model with the following Hamiltonian:

$$\mathcal{H} = \mathcal{H}_{\text{CEF}} - g_J \mu_{\text{B}} J_i H, \quad (4)$$

where \mathcal{H}_{CEF} is given by Eq. 2, the second term is the Zeeman term. The magnetization M_i is given by the following expression:

$$M_i = g_J \mu_{\text{B}} \sum_n |\langle n | J_i | n \rangle| \frac{\exp(-\beta E_n)}{Z}, \quad (i = x, y, z). \quad (5)$$

The calculated CEF magnetization is shown in Fig. 9(c) and (d) as solid lines. It is obvious from the figure that quantitatively the calculated CEF magnetization matches poorly with the experimental plots, which is tentatively attributed to the presence of Kondo interaction in these compounds. However, the calculated magnetization reflects the experimentally observed anisotropy. In the case of the rare-earth atom occupying the tetragonal site symmetry, the sign of the B_2^0 parameter usually determines the easy axis or easy plane of magnetization²⁸. Here the sign of B_2^0 is negative which indicates that [001] direction is easy axis of magnetization which is consistent with our experimental data.

Another estimate of the Kondo temperature has been obtained from the magnetic part of the heat capacity. In a typical Kondo lattice system, the magnetic part of the heat capacity can be thought to be the combination of the Kondo and Schottky contributions, which can be expressed as :

$$C_{4f} = C_K + C_{Sch}. \quad (6)$$

The expression for C_K is given by Schotte and Schotte²⁹ where they assumed a Lorentzian like density of states at the Fermi energy for the impurity spins $S = 1/2$:

$$C_K = k_{\text{B}} \frac{\Delta}{\pi k_{\text{B}} T} \left(1 - \frac{\Delta}{2\pi k_{\text{B}} T} \psi' \left(\frac{1}{2} + \frac{\Delta}{2\pi k_{\text{B}} T} \right) \right), \quad (7)$$

where ψ' is the first derivative of digamma function. Here Δ is the width of the Lorentzian and is assumed to be approximately the size of the Kondo energy $k_{\text{B}} T_K$. For a three level system C_{Sch} is given by the expression:

$$C_{Sch} = \left[\frac{R}{(k_{\text{B}} T)^2} \frac{e^{(\Delta_1 + \Delta_2)/k_{\text{B}} T} [-2\Delta_1 \Delta_2 + \Delta_2^2 (1 + e^{\Delta_1/k_{\text{B}} T}) + \Delta_1^2 (1 + e^{\Delta_2/k_{\text{B}} T})]}{(e^{\Delta_1/k_{\text{B}} T} + e^{\Delta_2/k_{\text{B}} T} + e^{(\Delta_1 + \Delta_2)/k_{\text{B}} T})^2} \right], \quad (8)$$

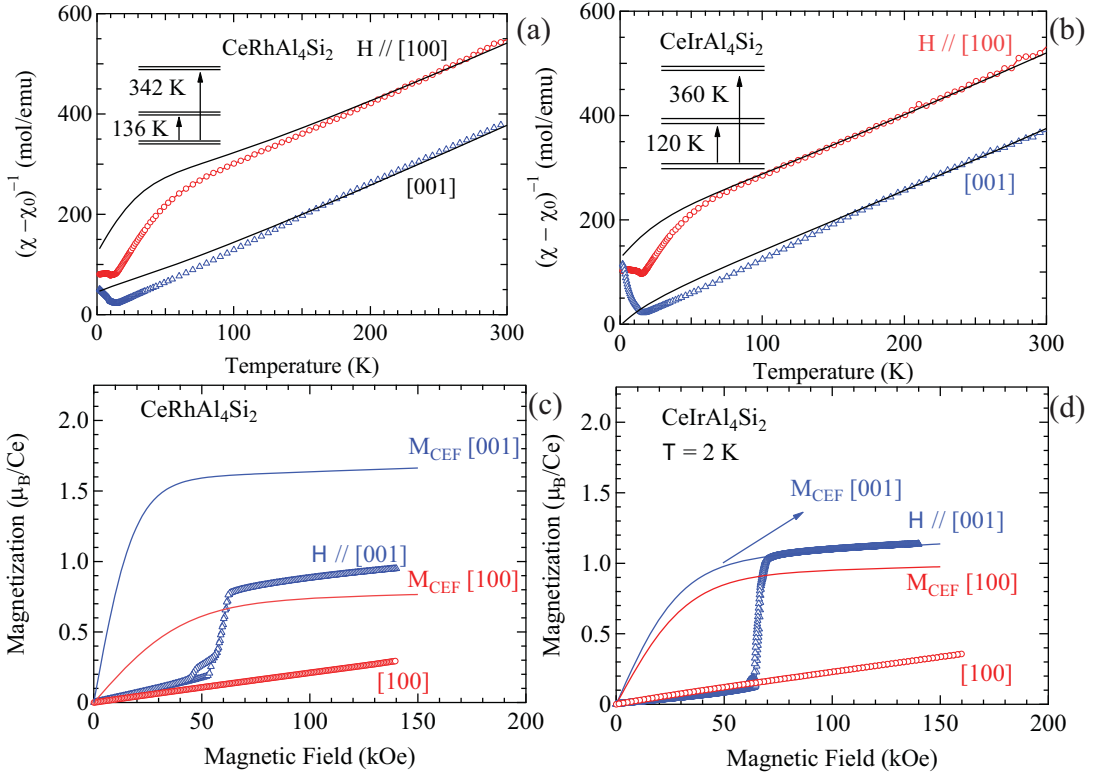


FIG. 9: (Color online) (a) and (b) Inverse susceptibility plot of $\text{CeRhAl}_4\text{Si}_2$ and $\text{CeIrAl}_4\text{Si}_2$ and the calculated CEF susceptibility. The CEF energy levels are also shown. (c) and (d) Isothermal magnetization measure at $T = 2$ K and the calculated magnetization curve based on the CEF model.

where R is the universal gas constant and Δ_1 and Δ_2 are the crystal field split excited energy levels. Using the energy levels obtained from the point charge model of the susceptibility data we have analyzed the magnetic part of the heat capacity using Eq. 6.

The solid line in Fig. 10 shows the combined contribution from the Kondo and the Schottky heat capacity, where the two contributions are calculated using Eq. 8 and Eq. 7, respectively. It is evident from the figure that the $4f$ -derived part of the heat capacity is reasonably well explained by Eq. 6. The Kondo temperature T_K thus obtained is 10-15 K for $\text{CeRhAl}_4\text{Si}_2$ and 5 K for $\text{CeIrAl}_4\text{Si}_2$, which are comparable to the values obtained using the procedure of Mori *et al.*¹⁸. A larger value of T_K implies a reduced jump in the heat capacity. If we refer to Fig. 10, the jump in the C_{4f} at the magnetic ordering temperature is smaller for $\text{CeRhAl}_4\text{Si}_2$ compared to that of $\text{CeIrAl}_4\text{Si}_2$ which has a lower T_K . Our crystal field calculations on the magnetic susceptibility and heat capacity data indicate that $\text{CeTAl}_4\text{Si}_2$ ($T = \text{Rh}$ and Ir) are Kondo lattice systems.

G. Electronic Structure

The local spin density approximation including Hubbard U -electron-correlation (LSDA+ U)³⁰ approach has been employed to investigate the electronic structure and magnetic properties of $\text{CeTAl}_4\text{Si}_2$ ($T = \text{Rh}, \text{Ir}$ and Pt) compounds. Calculations have been performed using the scalar relativistic version (which includes the mass velocity and Darwin correction terms) of the LSDA+ U method implemented in the tight binding linear muffin tin orbital (TB-LMTO)³¹ and full potential linear augmented plane wave (FP-LAPW)³² methods. We used $U = 6.7$ eV and $J = 0.7$ eV to model the onsite $4f$ -electron correlations of Ce atoms. Because of U the occupied spin up states move towards lower energy and the unoccupied spin down states move toward higher energy correcting the positioning of spin up occupied and spin down unoccupied $4f$ states that appear at the Fermi level from the bare LSDA calculations alone. The k-space integrations have been performed with $32 \times 32 \times 32$ Brillouin zone mesh which was sufficient for the convergence of the total energies (with accuracy of ~ 0.1 meV/cell) and magnetic moments (with accuracy of $0.01 \mu_B/\text{cell}$). The experimentally determined $P4/mmm$ crystal structure and lattice constants were used in these calculations.

Fig. 11 shows $4f$ and $5d$ density of states (DOS) of Ce

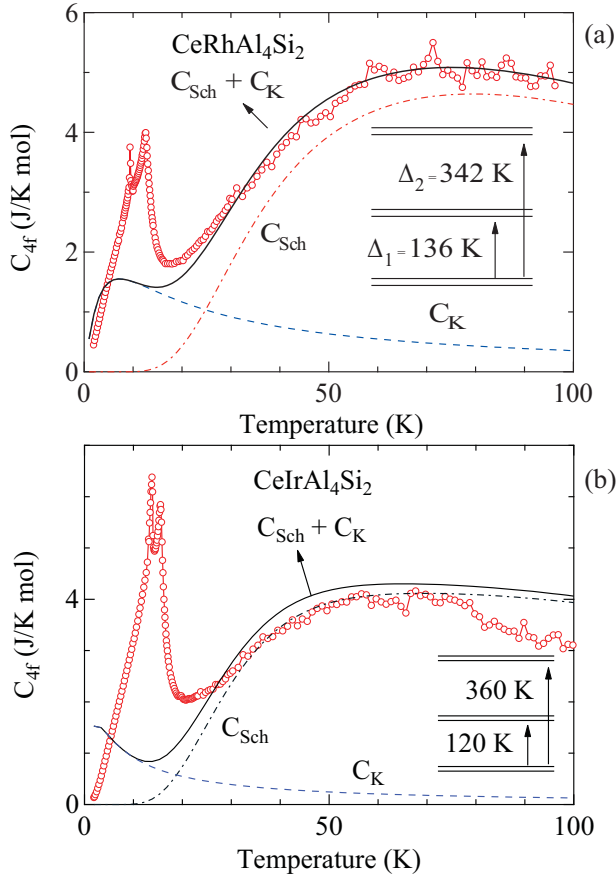


FIG. 10: (Color online) The $4f$ contribution to the heat capacity C_{4f} . The thick solid line is sum of the Kondo and Schottky contribution, dashed line is the Kondo contribution C_K and dashed-dotted line is due to the Schottky contribution C_{Sch} . The Schottky energy levels are also shown.

atoms in $CeTAl_4Si_2$ ($T = Rh, Ir,$ and Pt). The occupied spin up $4f$ DOS indicates two peaks and the unoccupied spin up DOS shows three peaks in both $CeRhAl_4Si_2$ (Fig. 11a) and $CeIrAl_4Si_2$ (Fig. 11b). However, the occupied spin up $4f$ states form single DOS peak in $CePtAl_4Si_2$ (Fig. 11c). Both $4f$ and $5d$ DOS curves rigidly shift towards the lower energy in $CeIrAl_4Si_2$ compared to $CeRhAl_4Si_2$. The rigid shift further increases in $CePtAl_4Si_2$. There is no spin polarization between the spin up and spin down $5d$ states in $CeRhAl_4Si_2$ (Fig. 11a) and $CeIrAl_4Si_2$ (Fig. 11b) which is possible only when $4f$ moments at two neighbouring Ce sites are antiparallel. However the $5d$ DOS in $CePtAl_4Si_2$ shows spin polarization between spin up and spin down $5d$ states (with $0.1 \mu_B$ of Ce $5d$) which is possible when $4f$ moments at two neighbouring Ce sites are parallel⁹. All the three compounds $CeRhAl_4Si_2$, $CeIrAl_4Si_2$, and $CePtAl_4Si_2$ compounds show identical $4f$ moment ($1.1 \mu_B$), which is comparable to the experimentally observed $4f$ local moment in these compounds. Furthermore, our calculations also indicate similar complex quasi-2D and nesting features of the Fermi surfaces in $CeTAl_4Si_2$ compounds

as obtained in $LaTAl_4Si_2$ counterparts (Ref. 9). Since the Ce $4f$ -states are away from the Fermi level, it is not surprising to obtain similar Fermi surface features in $CeTAl_4Si_2$ and the corresponding $LaTAl_4Si_2$ compounds. However, when treating Ce- $4f$ as delocalised bands, we find Fermi surface features very similar to $LaPtAl_4Si_2$ as pointed earlier in ref. 9. We note here that similar complex Fermi surface features and enhanced electronic coefficient of the specific heat have also been observed in Ce_2PdGe_3 ³³. Interestingly the total DOS at the Fermi level is higher by 19% in $CeRhAl_4Si_2$ compared to $CeIrAl_4Si_2$, which indicates a good trend with the observed coefficients of the electronic specific heat. As pointed out in ref. 33, the shapes of the Fermi surfaces may be reasonable but the mass renormalization, which is a dynamical entity, may not be fully captured in the electronic structure calculation.

The origin of the unusual physical properties, such as Kondo and heavy fermion behaviour, of some cerium compounds.^{34,35} is believed to be due to an unusual $4f$ density of states peak at the Fermi level³⁶ depending on the onsite electron correlations. The calculations with reduced Hubbard U parameter (e.g., for $U = 3$ eV) indicate that the double peak $4f$ DOS in $CeRhAl_4Si_2$ and $CeIrAl_4Si_2$ and single peak $4f$ DOS in $CePtAl_4Si_2$ (seen with $U = 6.7$ eV) shift towards the Fermi level (without significantly affecting the unoccupied $4f$ DOS) altering their coupling to the conduction electrons close to the Fermi level. Due to the formation of two $4f$ DOS peaks and low Ce $5d$ DOS in $CeRhAl_4Si_2$ and $CeIrAl_4Si_2$ there is a relatively weak hybridization between the $4f$ and the conduction electron states including Rh $4d$ /Ir $5d$ at the Fermi level. On the other hand, the formation of single $4f$ DOS peak and higher Ce $4f$ and $5d$ DOS in $CePtAl_4Si_2$ results in a slightly stronger hybridization between the $4f$ and the conduction electron states including Pt $5d$ at the Fermi level.

IV. CONCLUSION

We have successfully synthesized single crystals of $CeTAl_4Si_2$ ($T = Rh$ and Ir) by using the Al-Si binary eutectic composition as flux. The grown crystals have platelet like morphology with (001)-plane perpendicular to the plane of the crystal. Our comprehensive thermal and transport studies reveal that both compounds order antiferromagnetically with two Néel temperatures. A sharp metamagnetic transition is observed for $H \parallel [001]$ direction where as the magnetization is relatively small and varies linearly for $H \parallel [100]$ direction, indicating that [001] direction is the easy axis of magnetization in both the cases, which is consistent with neutron diffraction. A large negative paramagnetic Weiss temperature θ_p , a reduced magnetization, a reduced magnetic entropy and a negative logarithmic increase in the resistivity with decreasing temperature indicate that these compounds are Kondo lattice systems. The antiferromagnetic tran-

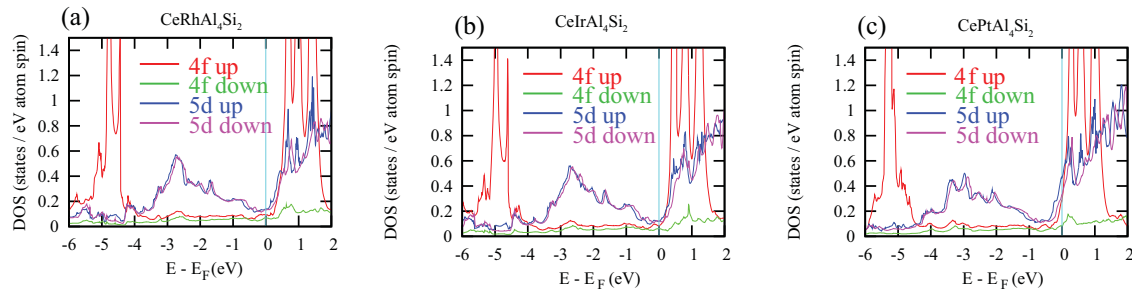


FIG. 11: (Color online) 4f and 5d density of states (DOS) of Ce atoms in $\text{CeTAl}_4\text{Si}_2$ ($T = \text{Rh, Ir, and Pt}$).

sition temperature decreases with pressure, confirming the presence of Kondo interaction in the two compounds. We have performed detailed crystal electric field calculations on the magnetization and heat capacity data and estimated the Kondo temperature and the energy levels of the $2J + 1$ degenerate ground state. It is found from our analysis that exchange interaction is anisotropic and the Kondo temperature is larger for Rh system. Our detailed electronic structure calculations provide an insight

into the observed magnetic and Kondo anomalies of these systems.

The electronic structure part of the work was supported by the U.S. Department of Energy, Office of Basic Energy Science, Division of Materials Sciences and Engineering. The Ames Laboratory is operated for the U.S. Department of Energy by Iowa State University under Contract No. DE-AC02-07CH11358.

-
- * Electronic address: sudesh@tifr.res.in
- ¹ A. Maurya, A. Thamizhavel, A. Provino, M. Pani, P. Manfrinetti, D. Paudyal and S. K. Dhar, *Inorg. Chem.*, **53**, 1443 (2014).
 - ² A. Maurya, P. Bonville, A. Thamizhavel and S. K. Dhar, arXiv:1411.0379v1 (2014).
 - ³ X. Wu and M. G. Kanatzidis, *J. Solid State Chem.*, **178**, 3233 (2005).
 - ⁴ S. E. Latturmer and M. G. Kanatzidis, *Inorg. Chem.*, **47**, 2089 (2008).
 - ⁵ B. Sieve, X. Chen, J. Cowen, P. Larson, S. D. Mahanti and M. G. Kanatzidis, *Chem. Mater.*, **11**, 2451 (1999).
 - ⁶ G. R. Stewart, *Rev. Mod. Phys.*, **56**, 755, (1984).
 - ⁷ N. Gerwe and F. Steglich, *Handbook on the physics and chemistry of rare earths*, North-Holland, Amsterdam **14**, p. 343 (1991).
 - ⁸ G. R. Stewart, *Rev. Mod. Phys.*, **73**, 4, (2001).
 - ⁹ N. J. Ghimire, F. Ronning, D. J. Williams, B. L. Scott, Y. Luo, J. D. Thompson and E. D. Bauer, *J. Phys.: Condens. Matter*, **27**, 025601 (2015).
 - ¹⁰ S. Doniach, *Physica B+C* **91**, 231 (1977).
 - ¹¹ N. J. Ghimire, S. Calder, M. Janoschek and E. D. Bauer, arXiv:1503.06860 (2015)
 - ¹² Juan Rodriguez-Carvajal, *Physica B* **192**, 55 (1993).
 - ¹³ J. D. Thompson 1993 *Selected Topics in Magnetism Vol.2* edited by L. C. Gupta and M. S. Multani (World Scientific) p.107.
 - ¹⁴ A. Maurya, P. Bonville, A. Thamizhavel and S.K. Dhar, *J. Phys.: Condens. Matter* **26**, 216001 (2014).
 - ¹⁵ J.M. Fournier and E. Gratz 1993 *Handbook on the Physics and Chemistry of rare earths: Transport properties of rare earth and actinide intermetallics vol.17* eds. K.A. Gschneidner, Jr. L. Eyring, G.H. Lander and G.R. Chopin (Elsevier Science Publishers) p409.
 - ¹⁶ V. Zlatic, *J. Phys. F* **11**, 2147 (1981).
 - ¹⁷ J.-P. Jan in *Solid State Physics*, vol.5, eds. F. Seitz and D. Turnbull (Academic Press Inc. New York 1957) p1.
 - ¹⁸ H. Mori, H. Yashima and N. Sato, *J. low. temp. phys.* **58**, 513, (1985).
 - ¹⁹ H. -U. Desgranges and K. D. Schotte, *Phys. Lett.* **91A**, 240, 1942.
 - ²⁰ M. T. Hutchings 1965 *Solid State Physics: Advances in Research and Applications Vol.16* edited by F. Seitz and B. Turnbull (New York: Academic) p.227.
 - ²¹ K. W. H. Stevens *Proc. Phys. Soc. (London)* **Sect.A65**, 209 (1952).
 - ²² P. K. Das, N. Kumar, R. Kulkarni and A. Thamizhavel, *Phys. Rev. B*, **83**, 134416 (2011).
 - ²³ A. Thamizhavel, R. Kulkarni and S. K. Dhar, *Phys. Rev. B*, **75**, 144426 (2007).
 - ²⁴ T. Takeuchi, S. Hashimoto, T. Yasuda, H. Shishido, T. Ueda, M. Yamada, Y. Obiraki, M. Shiimoto, H. Kohara, T. Yamamoto, K. Sugiyama, K. Kindo, T. D. Matsuda, Y. Haga, Y. Aoki, H. Sato, R. Settai and Y. Ōnuki, *J. Phys.: Condens. Matter*, **16**, L33 (2004).
 - ²⁵ K. Satoh, A. Fukada, I. Umehara, Y. Ōnuki, H. Sato, and S. Takayanagi, *J. Phys. Soc. Jpn.* **61**, 3267 (1992).
 - ²⁶ T. Takeuchi, A. Thamizhavel, T. Okubo, M. Yamada, N. Nakamura, T. Yamamoto, Y. Inada, K. Sugiyama, A. Galatanu, E. Yamamoto, K. Kindo, T. Ebihara, and Y. Ōnuki, *Phys. Rev. B* **67**, 064403 (2003).
 - ²⁷ T. Takeuchi, T. Inoue, K. Sugiyama, D. Aoki, Y. Tokiwa, Y. Haga, K. Kindo, and Y. Ōnuki, *J. Phys. Soc. Jpn.* **70**, 877 (2001).
 - ²⁸ A. Loidl, K. Knorr, G. Knopp, A. Krimmel, R. Caspary, A. Böhm, G. Sparr, C. Geibel, F. Steglich and A. P. Murani, *Phys. Rev. B* **46**, 9341 (1992).
 - ²⁹ K. D. Schotte and U. Schotte, *Phys. Lett.* **55A**, 38, (1975).

- ³⁰ V. I. Anisimov, F. Aryasetiawan, and A.I. Lichtenstein, J. Phys.: Condens. Matter. **9**, 767 (1997).
- ³¹ O. K. Andersen and O. Jepsen, Phys. Rev. Lett. **53**, 2571 (1984).
- ³² P. Blaha, K. Schwarz, G. Madsen, D. Kvasnicka, and J. Luitz, *WIEN2k*, An Augmented Plane Wave + Local Orbitals Program for Calculating Crystal Properties (Karlheinz Schwarz, Techn. Universitt Wien, Austria), ISBN 3-9501031-1-2 (2001).
- ³³ R.E. Baumbach, A. Gallagher, T. Besara, J. Sun, T. Siegrist, D.J. Singh, J.D. Thompson, F. Ronning and E.D. Bauer, Phys. Rev. B **91**, 035102 (2015).
- ³⁴ W. E. Pickett and B. M. Klein, Journal of the Less-Common Metals, **93**, 219 (1983).
- ³⁵ T. Jarlborg, A. J. Freeman, and D. D. Koelling, J. Magn. Mater **60**, 291 (1986).
- ³⁶ T. Jarlborg, A. J. Freeman, and D. D. Koelling, J. App. Phys. **53**, 2140 (1982).